International Journal of Nanoscience
Vol. 9, No. 4 (2010) 311–315

DOI: 10.1142/S0219581X10006867

World Scientific
www.worldscientific.com

NANOSCALE ARRAYS IN LITHIUM NIOBATE FABRICATED BY INTERFERENCE LITHOGRAPHY AND DRY ETCHING

G. Y. SI and A. J. DANNER*
Department of Electrical and Computer Engineering
National University of Singapore, 4 Engineering Drive 3
Singapore 117576, Singapore
**adanner@nus.edu.sg*

J. H. TENG†, S. S. ANG and A. B. CHEW
Institute of Materials Research and Engineering
3 Research Link, Singapore 117602, Singapore
†*jh-teng@imre.a-star.edu.sg*

E. DOGHECHE
Institut dElectronique Microelectronique Nanotechnologie
IEMN CNRS LCI, Avenue Poincaré, 59652 BP60069
Villeneuve d'Aseq, France

Channel waveguides have been fabricated in x-cut lithium niobate ($LiNbO_3$) by proton exchange (PE) method and optically measured. The thickness and the optical constants of the thin PE layer were characterized using a prism coupling technique. The PE area was plasma etched and a 2.775-μm total etching depth was achieved. The measured average etching rate is 92.5 nm/min. One- and two-dimensional dense arrays of $LiNbO_3$ nanostructures have also been fabricated by using interference lithography (IL) and inductively coupled plasma reactive ion etching (ICP-RIE) techniques.

Keywords: $LiNbO_3$ dense arrays; plasma etching; interference lithography.

1. Introduction

Lithium niobate ($LiNbO_3$) has drawn much attention because of its peculiar optical properties, such as electro-optic, acousto-optic, and piezoelectric effects. Conventionally, a waveguide in $LiNbO_3$ crystal is fabricated using metal diffusion, ion exchange, or proton exchange (PE). Compared with the common Ti in-diffusion method, the PE process has a much higher photorefractive damage threshold for guiding a visible laser.[1] Furthermore, many proton sources have been used in the PE process, including benzoic, adipic, stearic, octanoic, and glutaric acids and their mixtures.[2–4] Waveguides in $LiNbO_3$ are used for high-speed modulation or for nonlinear devices such as parametric oscillators and amplifiers. $LiNbO_3$ is also common in telecommunication systems due to its high electro-optic

*Corresponding author.

coefficient and low optical losses. In addition, the fabrication of $LiNbO_3$ photonic crystals[5–7] could find applications in decreasing the size of some crucial components in many optical systems. However, it is very difficult to etch $LiNbO_3$ due to its poor reactivity with common etchants and selectivity issues. There are two normal ways of $LiNbO_3$ etching, wet etching and plasma etching. Wet etching is a frequently used processing step but is seldom applied to $LiNbO_3$ because of the material's strong etch resistance which results in low etch rates and sometimes nonuniform etching.[8–10] Introduction of structural defects can speed up the etching considerably, therefore the combinations of ion bombardment and subsequent wet etching have been demonstrated as a useful method for etching of $LiNbO_3$. For plasma etching, the main limitation is the redeposition of LiF which will lower the etching rate when fluorine gases are involved. To improve this, a proposed way is using the mixture of fluorine gases with argon or oxygen. Previously, a maximum etching rate without cooling of 5.7 μm/h was obtained with CHF_3/Ar.[11] Most recently, an optimized SF_6/Ar mixture was applied to provide etching rates of up to 190 nm/min.[12]

In this paper, we report the fabrication of a channel waveguide and the optical measurement of the PE layer. Afterward, a trench was formed in the PE area by plasma etching. The side view shows a nearly vertical profile and the measured etch rate is 92.5 nm/min. We also demonstrate the fabrication of nanometric-sized arrays of gratings and rods with a 260-nm period. The PE process reduces the concentration of lithium (Li) ions, which makes both vertical channel profiles and uniform nanoarrays realizable.

2. Fabrication Details and Measurement

2.1. *Channel waveguide fabrication*

The fabrication procedure is as follows. First, a 5-μm-wide strip pattern was defined on the x-cut $LiNbO_3$ substrate by photolithography. Then, chromium (Cr) of 50-nm thickness was deposited on the surface of the sample by electron-beam evaporation. Subsequently, Cr and photoresist in the strip area were removed by a lift-off process. After that, the wafers were fully immersed in molten benzoic acid at 235°C for PE for 3 h and finally they were cut and facet-polished for test.

2.2. *Optical measurement of waveguide*

To measure the thickness and the optical properties of the PE $LiNbO_3$ layer, a prism coupling technique was applied. A laser beam with 633 nm wavelength was coupled into the structure by a rutile prism with an angle of 43°. From knowledge of the effective mode indices, the refractive index profile can be determined as a function of the film thickness for either TE or TM modes. With a certain incidence angle to the prism normal, either TE or TM-polarized modes will be coupled into the film. The guided modes will propagate inside the PE layer with an effective refractive index between that of bulk substrate and the PE layer. From the angular position of the guided modes, the corresponding effective indices and hence the refractive indices and the film thickness can be computed. This method has been widely used as a powerful tool to investigate the optical characteristics of different kinds of thin films because it can provide information on both the thickness and refractive index of various layers in multilayered structures. By measuring the reflected intensity from the prism as a function of the incident angle, we can find the guided TE modes as dips in the reflection spectrum. The refractive index is calculated through the TE mode data and through use of the well-known guided-mode dispersion equations for a planar waveguide. Figure 1 shows the reflection intensity of the sample after 3 h PE as a function of the incident angle. Four guided modes have been excited. The sharpness of the reflectivity dips indicates a good confinement of the light into the waveguide. As we can see from the plot, the excited mode at a $\sim 29°$ coupling angle

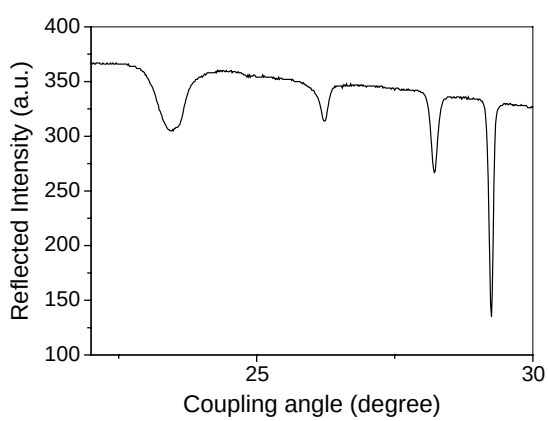

Fig. 1. Guided-mode spectrum as a function of incident angle.

has a sharper profile than the other three, which indicates better light confinement. The calculated waveguide depth is 2.4361 μm with 2.303 ordinary refractive index.

To characterize the performance of the channel waveguide, a laser with 1550 nm wavelength was coupled into the device using a lensed fiber with a tip diameter of 2.5 μm. The waveguide output was captured by an infrared charge-coupled device (CCD) camera through an objective lens. Figure 2 shows the measured mode profile of a 3 h PE processed $LiNbO_3$ channel waveguide. The mode size is an important parameter particularly for nonlinear optics applications. The remote inhomogeneity shown in the intensity distribution is due to possible imperfect facets during dicing and polishing.

2.3. *Plasma etching of the channel waveguide*

Finally, plasma etching was carried out to remove the PE area with Cr acting as mask. CHF_3/Ar (flow rate 50/50) was used as recipe at 20 mTorr chamber pressure. Argon was added to mix with CHF_3 in order to enhance the physical component during etching and thereby achieve a better profile. The ICP source rf power was 500 W and the RIE power was set up to 250 W. After etching for 30 min, the samples were cooled down at 25°C and taken out of the ICP chamber. Then the Cr layer was removed by wet etching.

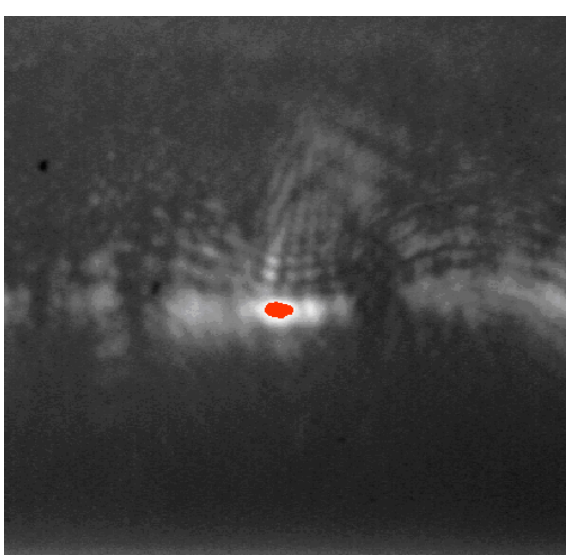

Fig. 2. Measured optical near-field mode profile of a channel waveguide after 3 h PE.

2.4. *Nanogratings and nanorods fabrication*

The channel etching result demonstrates the potential of obtaining uniform structures in $LiNbO_3$ after a PE process. Structures of grating or rod arrays at the nanometer scale could find application in photonic devices. Therefore, we have also developed a fabrication process for large-area dense arrays of $LiNbO_3$ nanogratings and nanorods using interference lithography (IL) and ICP etching techniques. IL can define one- and two-dimensional arrays by exposing laser beams one or two times to the sample with positive or negative photoresist on the surface. Additionally, one can control the geometry of the arrays in a wide range by changing the processing parameters such as incident angle and exposure time. In this work, positive resist S1805 was spun onto x-cut $LiNbO_3$, followed by IL with a 325-nm UV source (a helium cadmium laser) to define arrays of gratings or rods in the resist at a period of 260 nm. Finally, the samples were plasma etched for 90 sec using the same etching parameters mentioned above and the resist was removed by acetone after etching.

3. Results and Discussion

The cross-sectional scanning electron microscopy (SEM) image of the etched trench profile is shown in Fig. 3. The measured etching rate is 92.5 nm/min (2.775-μm etching depth for 30 min etching time). Many different techniques have been investigated to etch $LiNbO_3$. However, it is really difficult to overcome the underetching problem using a wet etching method[8–10] and the cone-shaped structure

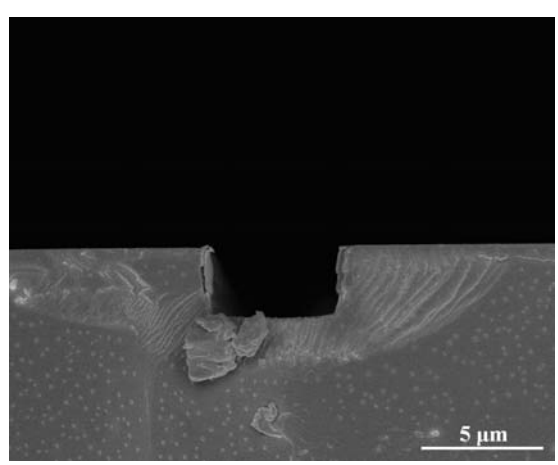

Fig. 3. SEM picture of the etched trench cross-section.

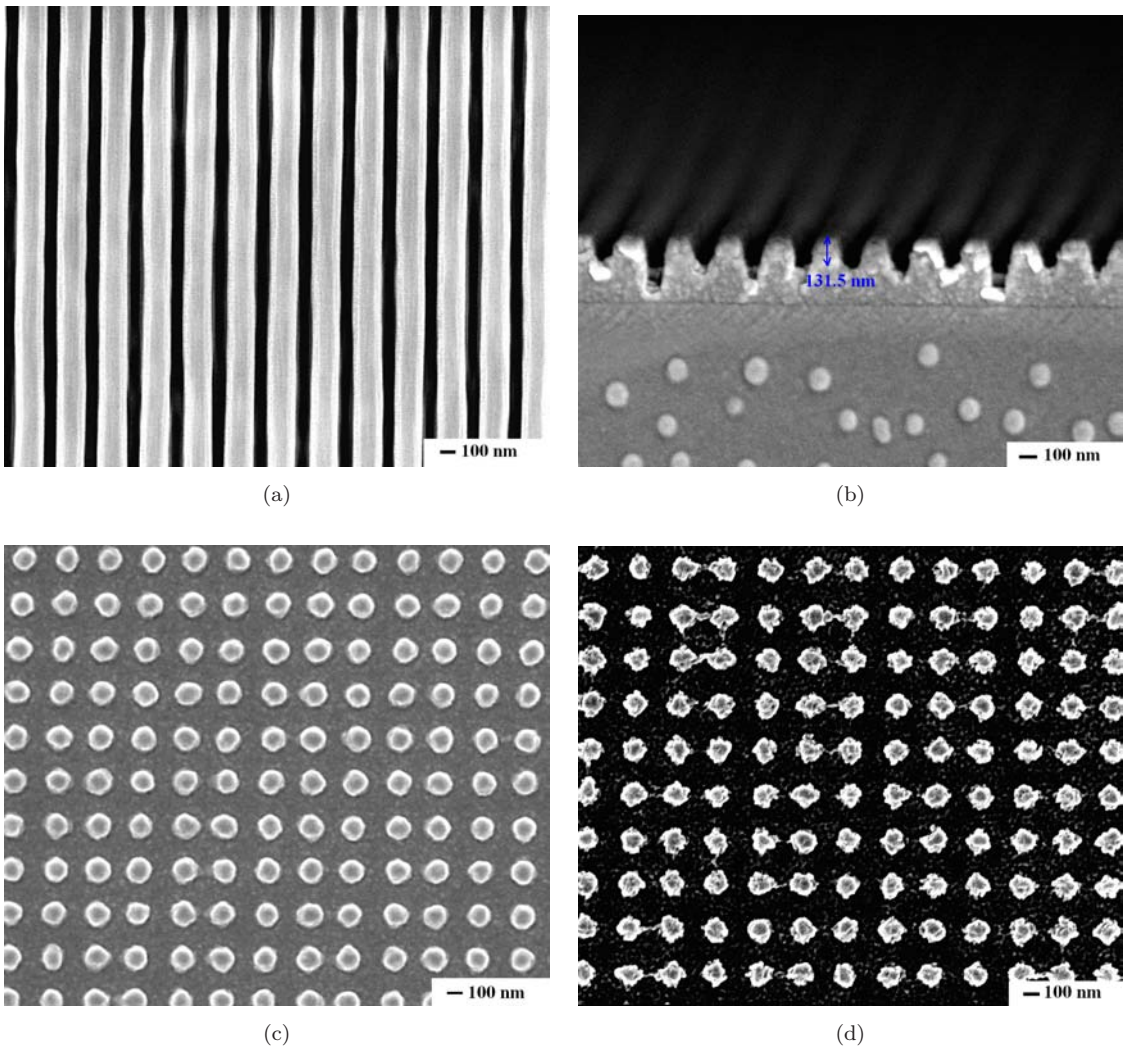

Fig. 4. SEM pictures of: (a) top view and (b) side view of the grating array. (c) Top view of the nanorod array before and (d) after plasma etching.

when focused ion beam is used for photonic crystal milling.[5]

The top view and the side view of the fabricated grating nanoarrays are illustrated in Figs. 4(a) and 4(b), respectively. The measured grating depth is 131.5 nm (highlighted by a blue arrow) which corresponds to an etching rate of 87.7 nm/min, a little smaller than the measured deep trench etching rate. CHF_3 was used in this work because it is superior to CF_4 in dry etching of $LiNbO_3$ due to suppressed deterioration of the surface. Figure 4(c) shows the top view of the resist nanorods after IL pattern definition and before etching. In Fig. 4(d), the plane view of the transferred pattern from resist into the $LiNbO_3$ substrate is demonstrated. It is evident that resist surface is smooth and the pattern is uniform. Photoresist was acting as a selective mask during plasma etching.

Contrastively, there are tiny spots interspersing on the sample surface after plasma etching, as shown in Fig. 4(d). This is because of the redeposition of LiF during etching. Although the concentration of Li ions was reduced significantly (replaced by an equal number of protons) compared to original $LiNbO_3$ after PE which therefore could result in a decreased LiF redeposition rate, there was still LiF formed during dry etching due to the involvement of a fluorine-containing recipe.

4. Conclusion

In summary, we have fabricated a channel waveguide with good optical confinement and measured the PE thin layer. In addition, a trench with almost vertical sidewall was obtained in the PE area by ICP etching. We have also demonstrated the fabrication

of high-density grating and rod arrays with nanometer scale in x-cut $LiNbO_3$ by combining the IL technique and plasma etching. The results offer a potential approach of deep and vertical etching profiles of $LiNbO_3$ nanostructures, which could find applications in integrated optical devices.

References

1. T. Fujiwara, R. Srivastava, X. Cao and R. V. Ramaswamy, *Opt. Lett.* **18**, 346 (1993).
2. K. Ito and K. Kawamoto, *Jpn. J. Appl. Phys.* **31**, 3882 (1992).
3. V. M. N. Passaro, M. N. Armenise, D. Nesheva, I. T. Savatinova and E. Y. B. Pun, *J. Lightwave Technol.* **20**, 71 (2002).
4. W. J. Liao, X. Chen, F. Chen, Y. Chen, Y. Xia and Y. Chen, *Opt. Laser Technol.* **36**, 603 (2004).
5. M.-P. Bernal, N. Courjal, J. Amet, M. Roussey and C. H. Hou, *Opt. Commun.* **265**, 180 (2006).
6. M. Roussey, M.-P. Bernal, N. Courjal and F. I. Baida, *Appl. Phys. Lett.* **87**, 241101 (2005).
7. M. Roussey, M.-P. Bernal, N. Courjal, D. Van Labeke, F. I. Baida and R. Salut, *Appl. Phys. Lett.* **89**, 241110 (2006).
8. T.-J. Wang, C.-F. Huang, W.-S. Wang and P.-K Wei, *J. Lightwave Technol.* **22**, 1764 (2004).
9. T.-L. Ting, L.-Y. Chen and W.-S. Wang, *IEEE Photonics Technol. Lett.* **18**, 568 (2006).
10. H. Hu, R. Ricken, W. Sohler and R. B. Wehrspohn, *IEEE Photonics Technol. Lett.* **19**, 417 (2007).
11. H. Hu, A. P. Milenin, R. B. Wehrspohn, H. Hermann and W. Sohler, *J. Vac. Sci. Technol. A* **24**, 1012 (2006).
12. Z. Ren, P. J. Heard, J. M. Marshall, P. A. Thomas and S. Yu, *J. Appl. Phys.* **103**, 034109 (2008).